Ferromagnetic Nanoparticles Dose Based on Tumor Size in Magnetic Fluid Hyperthermia Cancer Therapy

M. Pavel[1,2] and A. Stancu[2]

[1]Physics Department, "Alexandru Ioan Cuza" University, Iasi 700506, Romania
[2]"Gr. T. Popa" University of Medicine and Pharmacy, Iasi 700115, Romania

The interest in magnetic fluid hyperthermia (MFH) and cancer therapy has noticeably increased in the last years. At present, a successful realization of this interdisciplinary research is hampered by some unsolved problems. One of these problems this paper intended to clarify is how to find an estimate of the appropriate dosage of magnetic nanoparticles that injected into the tumor would help achieve an optimum temperature of 42°C, thus resulting in an increase of the susceptibility for apoptosis in tumor cells. We created a computational model in COMSOL: Multiphysics in order to analyze the heat dissipation within the tumor tissue. By considering various types of tissues with their respective physical and physiological properties (breast, liver, and skin tissues) and also by taking into account the amount of heat generated through the Brownian rotation and the Néel relaxation, it has been studied the tumor border temperature achieved for various concentrations of magnetic nanoparticles in their superparamagnetic behavior. Distinct simulations of a spherical tumor located in a cubical region of a volume of 1.2–3.5 cm^3 within the tissue were designed. We performed a systematical variation of tumor diameter and particle dosage for every physical parameter of above mentioned tumor tissues (e.g., tissue density, tumor/tissue perfusion rate). By this systematization we intended to understand the interdependence of these parameters and their effects on hyperthermia therapy.

Index Terms—**Bioheat equation, hyperthermia, magnetic nanoparticles dose, perfusion rate, tumor.**

I. Introduction

THE power of healing by heat generation has been well known for a very long time and used in the treatment of many diseases. The concept of inducing hyperthermia locally into the tumor is not new. It is known as an innovative form of cancer therapy among the classical methods such as irradiation, surgery, or chemotherapy. This method is based on the principle that temperatures higher than 42°C may induce apoptosis in cancer cells while the normal cells are not affected and may survive due to different mechanisms of thermoregulation [1], [2]. Although, there has not yet been clarified an effective and safe limit of the temperatures achieved during the hyperthermia treatment within the tissue.

The benefits of the external alternating electromagnetic field effects on magnetic nanoparticles less than 200–300 nm in size, was first described by the Gordon *et al.* [3]. Among magnetic materials, magnetite, Fe_3O_4 is one of the most commonly used in different fields of biomedicine and biotechnology due to its heating capabilities, low toxicity and good biocompatibility [1], [4].

Apart from the theoretical aspects discussed above there are still numerous problems that need to be solved before the proceeding of a clinical model. Ones of the major points that have not been yet established for MFH are the generation and the control of a well defined heating field at the tumor. In this case, the challenge is to quantify the optimum dose of magnetic material that injected into the tumor would lead to a therapeutic temperature of at least 42°C and limit the heating area to the tumor as precisely as possible.

It is well known that the heating of these particles in an AC-magnetic field is mainly due to three loss processes: hysteresis losses, relaxation losses, and resonance losses [4], [5]. As resonance loss occurs at very high frequency, it may be neglected for MFH applications. The hysteresis loss results from the hysteretic properties of magnetic materials exposed to a time varying magnetic field and may be estimated from the area of the hysteresis loop, taking into consideration the proportionality of the power loss to frequency. The amount of heat generated per unit volume in the ferromagnetic (FM) regime is given by multiplying frequency with the area of the hysteresis loop [6]:

$$\mathrm{LP_{FM}} = \mu_0 f \oint H dM \tag{1}$$

where permeability $\mu_0 = 4\pi \cdot 10^{-7}$ H/m.

The relaxation processes may occur through one of the two distinct mechanisms: Brownian and Néel relaxation, effects that are taken into account by considering the effective relaxation time τ_R. The loss power achieved in these conditions corresponds to the superparamagnetic (SPM) regime [2], [5], [7]:

$$\mathrm{LP_{SPM}} = \mu_0 \pi \chi_0 f \frac{2\pi f \tau_R}{1 + (2\pi f \tau_R)^2} H^2. \tag{2}$$

In this equation $\chi_0 = \mu_0 M_S^2 V/(k_B T)$, M_S is the saturation magnetization, V is the particle volume, and k_B is the Boltzmann constant. The effective relaxation time is given by $\tau = (\tau_N \cdot \tau_B)/(\tau_N + \tau_B)$, where τ_B and τ_N are the Brownian and Néel relaxation time, respectively [2], [5]. The Brownian relaxation time depends on the viscosity coefficient (η) of the fluid and the hydrodynamic volume of the particle (V_H) as it follows: $\tau_B = (3\eta V_H)/(k_B T)$ [2], [5]. The Néel relaxation time of the system is determined by the ratio of anisotropy energy KV to thermal energy $k_B T$: $\tau_N = \tau_0 \exp[\mathrm{KV}/(kT)]$ with $\tau_0 \sim 10^{-9} s$ [5].

The field frequency and amplitude used to generate the heating area are limited by biomedical reasons. The alternating electromagnetic field causes not only the therapeutic useful

Manuscript received July 16, 2009. Current version published October 23, 2009. Corresponding author: M. Pavel (e-mail: pmariana@stoner.phys.uaic.ro).

Color versions of one or more of the figures in this paper are available online at http://ieeexplore.ieee.org.

Digital Object Identifier 10.1109/TMAG.2009.2031076

heating effect of the magnetic particles, but also the heating of both cancerous and healthy tissues. In this direction, Brezovich concluded that exposure to fields with $H \cdot f \leq 4.85 \times 10^8$ $\mathrm{Am^{-1}\ s^{-1}}$ is safe and tolerable [8]. But, taking into account the aim of using MFH, Hergt and co. assumed a weaker criterion with $\mathrm{C} = 5 \times 10^9$ $\mathrm{Am^{-1}\ s^{-1}}$, where $\mathrm{H} \cdot \mathrm{f} < \mathrm{C}$ [9].

II. Computer-Based Model of Heat Transfer in Biological Tissues

By taking into account the biocompatibility criterion mentioned above, we concluded in a previous paper [10] that loss power should be less than 7.5×10^9 W/m^3, values that correspond to a field amplitude less than 7 kA/m and field frequency less than 250 kHz when considered particles of 18 nm in diameter (with a superparamagnetic behavior) and to field amplitude and frequency less than 15 kA/m and respectively 500 kHz for particles that describe a hysteretic behavior. We have also concluded the benefits of magnetite magnetic material and we advanced our simulations by taking into account the physical properties of magnetite.

Finite element method (FEM) simulations were performed by using COMSOL Multyphysics (Heat Transfer Module) in order to simulate the heat dissipation into the cancer and normal tissues.

The transfer of thermal energy in living tissues is a complex process which involves both metabolic heat and blood flow. The interaction between the blood perfusion rate through the vascular network on the local temperature distribution and other physiological processes such as inflammation and thermoregulation influences in different ways the bioheat transport into the body. For example, the blood flow within the tissue is increased by thermoregulation in order to remove the heat supply. The equation that best describes the heat transport within the tissue is Pennes' bioheat equation which combines the contribution of blood perfusion rate, heat conduction, and the amount of energy generated by the metabolic processes [11], [12]:

$$\delta_{tz}\rho c\frac{\partial T}{\partial t}+\nabla\cdot(-k\nabla T)=\rho_b c_b\omega_b(T_b-T)+Q_{\mathrm{met}}+Q_{\mathrm{ext}} \quad (4)$$

where ρ is the tissue density, c is the tissue specific heat, ρ_b is the density of blood, approximated with 1000 kg/m^3, c_b is the blood' specific heat, 4180 J/(kg·K), k is the tissue thermal conductivity, 0.512 W/(m·K), ω_b is the blood perfusion rate, T_b is the arterial blood temperature, approximated as the core temperature of the body—310.15 K [11], [12], T is the local temperature, Q_{met} is the metabolic heat source, which for skin is 400 W/m^3, for glandular tissue is 700 W/m^3 and for cancerous tissue is 5790 W/m^3 [13], and Q_{ext} is the heat generated by loss power.

For magnetite we considered the heat capacity of 670 J/(kg·K) and the density of 5180 kg/m^3. The physical and physiological properties of the tissues analyzed are presented in Table I.

Based on the results we have obtained in a previous paper [10], we designed different simulations of a spherical tumor located in various tissues. Another correlated study to the one presented in this paper was presented at the Intermag Conference in 2009, where the case of heating multiple micrometastases located in different body regions was analyzed [18]. By using COMSOL Multiphysics Module, we intended to compute the spatial temperature distribution within the tissues. We have considered three possible situations.

TABLE I
Physical and Physiological Properties

Quantity	Breast	Liver	Skin	Reference
Tumor Density (kg/m^3)	1060	21500	1160	[11], [14]
Tissue Density (kg/m^3)	980	1060	1050	[14] - [16]
Tumor Perfusion Rate (1/s)	0.01333	0.0064	0.0135	[11], [13], [17]
Tissue Perfusion Rate (1/s)	0.00667	0.0064	0.00833	[11], [13], [16]
Tumor Heat capacity (J/(kg·K))	2300	132	1730	[11], [16]
Tissue Heat capacity (J/(kg·K))	2300	3600	1730	[11], [16]
Tumor Thermal conductivity (W/(m·K))	0.57	71	0.512	[11], [14]
Tissue Thermal conductivity (W/(m·K))	0.57	0.512	0.512	[11], [14]

Physical and physiological properties of the tumor and healthy tissues.

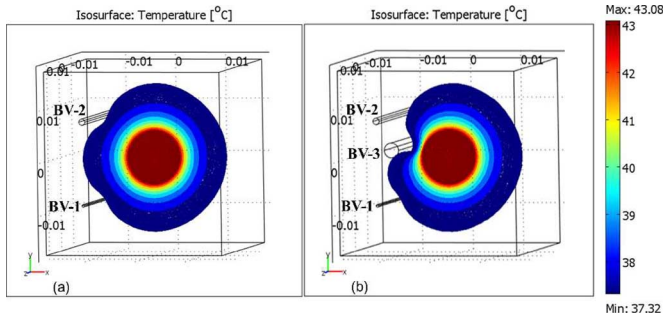

Fig. 1. Spatial temperature distribution in a skin tissue tumor (a) First Model described (b) Second Model described. Conditions: LP $= 1.1 \times 10^9$ W/m^3 and concentration of nanoparticles $= 5$ mg/cm^3.

The first model designed in this study was approximated by using a cubical region of a volume of 42.875 cm^3 (3.5 cm $\times$ 3.5 cm $\times$ 3.5 cm). Two blood vessels with a diameter of 0.5 mm and 1.2 mm respectively were located at 7.5 mm each from the tumor border. The tumor was configured as a perfect sphere with a diameter that varied from 1 to 1.6 cm, depending on the simulation.

In the second model computed, we assumed the presence of one blood vessel more of 2.8 mm in diameter, near to the tumor region at 1–2 mm distance from it, in order to study the influence of blood constant systemic temperature on the heat dissipation into the tissues. These aspects may be observed in the Fig. 1. In the first two models already mentioned, the magnetic nanoparticles of magnetite were concentrated in multiple small regions (of 0.9 mm diameter) inside the tumor, homogenously distributed around its border. The physical and physiological properties of the breast, liver and skin tissues used in these simulations are presented in Table I. There were no particles in the

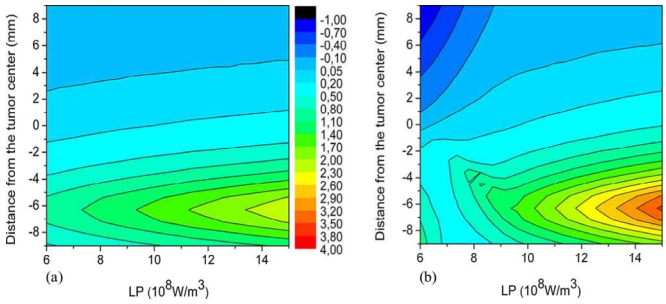

Fig. 2. The temperature differences (°C) between the results obtained in the piece of breast tissue considered when computing the first two models for different concentrations of nanoparticles: (a) 5 mg/cm^3 (b) 8 mg/cm^3. The negative axis corresponds to the tissue region next to the blood vessel of 2.8 mm.

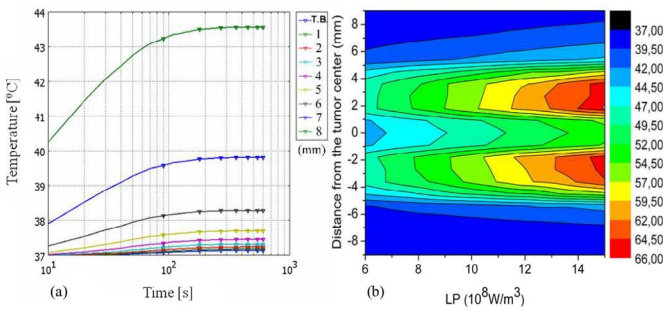

Fig. 3. (a) The variation in temperature over time (°C)—expressed in log scale, at different distances from the tumor border in the breast tissue for the second model presented. (b) The temperature distribution (°C) within breast tissue for the second model presented. The conditions involved in both cases are: LP $= 1 \times 10^9$ W/m^3 and concentration of nanoparticles $= 5$ mg/cm^3. The negative axis corresponds to the tissue region next to the blood vessel of 2.8 mm.

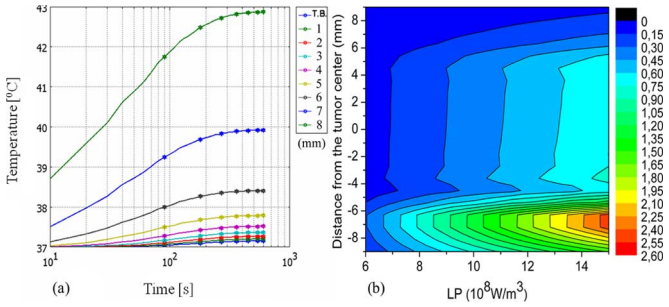

Fig. 4. (a) The variation in temperature over time (°C)—expressed in log scale, at different distances from the tumor border in the liver tissue for the second model presented. (b) The temperature differences (°C) between the results obtained in the piece of liver tissue considered when computing the first two models. The conditions involved in both cases are: LP $= 1 \times 10^9$ W/m^3 and concentration of nanoparticles $= 5$ mg/cm^3. The negative axis corresponds to the tissue region next to the blood vessel of 2.8 mm.

center of the tumor, aspect that may be observed in the next figures. The dosage of nanoparticles was varied from 3 up to 12 mg/(cm^3 of tumor tissue). For therapeutic LP values we have chosen a range between $(0.6\text{–}1.4) \times 10^9$ W/m^3.

In the third model, our next attempt was to estimate the variation of tumor border temperature when the tumor diameter is varied for different concentration of magnetic material and different loss power. In this case a smaller spherical tumor was located in a cubical region of volume 1 cm^3 from the breast tissue. The particles were randomly concentrated in 6 regions of 0.9 mm diameter each inside the tumor area and the nanoparticles concentration was varied from 6 up to 13 mg/cm^3. In order to achieve the optimum temperature value of 42°C, a higher range of LP values has been chosen: $(3.4\text{–}6.0) \times 10^9$ W/m^3.

III. Results and Discussions

In all our simulations we have assumed a monodispertion distribution of magnetic nanoparticles. The size polydispersity, which is present in all real nanoparticles, limits the specific loss power that can be obtained [19]. Nevertheless, by choosing appropriate alternating electromagnetic field parameter values in order to achieve the respective loss power specified in our models, the heat distribution area within the tissues is estimated.

The first two simulations show the heat dissipation that takes place in breast, liver and respectively skin tumors surrounded by healthy tissues. Firstly, we were interested in observing the blood vessels' effect when it is very close to the tumor (1–2 mm distance from it). In order to establish this effect we compared the results achieved from the first two models and we concluded that in the case of liver and breast tissue the presence of a blood vessel near to the tumor has an increased influence on the heat dissipation. Moreover, this effect it is better observed for increased values of loss power. All these aspects are represented in Figs. 2–4, where the negative axis corresponds to the tissue region next to the blood vessel of 2.8 mm. Further blood vessels, positioned at 7 mm away from the tumor border, have only a slight influence on the heat dissipation within the tissue. When using tumors models of the order of centimeters, in comparison with smaller ones (on a millimeter scale) [10], the therapeutic temperature is achieved by using o smaller dose of nanoparticles per cm^3 of tumor tissue at lower values of external applied field parameters.

For example, in the case of skin tissue, for a tumor of 3–4 mm in diameter a therapeutic result is achieved for a concentration of nanoparticles of 6 mg/cm^3 and LP values between $(4.2\text{-}4.8) \times 10^9$ W/m^3 [10]. In comparison, for a larger tumor of more than 1 cm in diameter, similar temperature values are obtained at a lower dose of nanoparticles (less than 5 mg/cm^3) and lower external applied field features (LP values of $(0.8\text{-}0.9) \times 10^9$ W/m^3).

The local features (tissue density and tissue perfusion rate) may have an important influence on the temperature variation in time. When the physical and physiological properties of the tumor are very different from the local ones, the temperature distribution suffers an important influence from the blood vessels closely located to the tumor. More specifically, an increase in the tumor density and tumor thermal conductivity leads to a faster temperature variation in time, but in the same time the tumor border temperature achieved is smaller. This aspect is revealed by comparing Fig. 3(a) (a slight difference between the tumor and normal tissue features) with Fig. 4(a), where a large variation between the tumor and tissue parameters is seen. The presence of a blood vessel near to the tumor drastically reduces the temperature achieved in the tissue in comparison with the case when no large blood vessels are located around the tumor [see Fig. 4(b)].

In the case of the skin tissue the optimal temperature at the tumor border (Fig. 5) is obtained by choosing a lower concentration of magnetic material and lower field features, in contrast with the other two types of tissues studied.

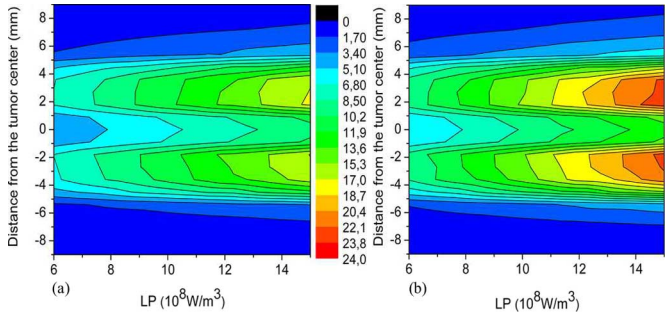

Fig. 5. The temperature differences (0°C) between the results obtained in the piece of skin tissue considered when two concentrations of nanoparticles are used in the second model described: (a) 8 mg/cm^3 and 5 mg/cm^3 (b) 12 mg/cm^3 and 8 mg/cm^3. The negative axis corresponds to the tissue region next to the blood vessel of 2.8 mm.

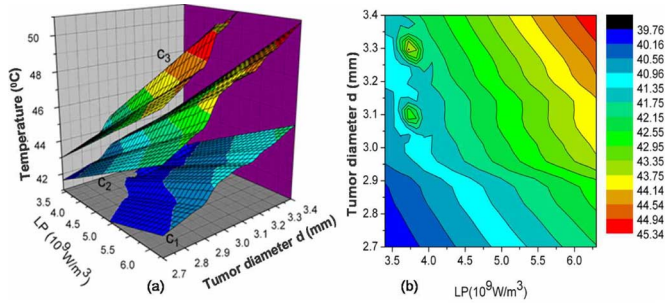

Fig. 6. (a) Tumor border temperature (°C) within a breast tissue for different concentrations of magnetic nanoparticles when the third model is computed: $C1 = 6$ mg/cm^3, $C2 = 10$ mg/cm^3, $C3 = 13$ mg/cm^3. (b) The temperature dependence (°C) on tumor diameter and LP value at a concentration of nanoparticles of 6 mg/cm^3.

We further simulated the heat dissipation for the second model presented by varying the tumor diameter from 1 to 1.6 cm. We observed that in the same conditions (LP values) the temperature achieved to the tumor border for this range of size does not suffer a noticeable change. By increasing both the value of the field frequency and amplitude, which implies an increasing in the LP value, and the concentration of nanoparticles, the temperature suffers a sudden variation within the tissue.

For the third simulation, we assumed breast tissue where the tumor diameter from 2.7 up to 3.4 mm for different concentrations of nanoparticles (6, 10, and respectively 13 mg/cm). Small temperature variations when the tumor diameter increases may be achieved for values of LP less than $(4.5–5.0) \times 10^9$ W/m^3 (Fig. 6). In comparison with larger breast tumors (larger than 1 cm diameter), when using the same concentration of nanoparticles, similar tumor border temperatures are achieved for lower LP values (less than 1.0×10^9 W/m^3) that imply a decrease in the field frequency and field amplitude, respectively.

IV. Conclusion

One of the most challenging unsolved problems in MFH is the choice of the right dose of nanoparticles and the optimum applied field parameters in order to achieve the desired temperature of 42°C within a specified region inside the body. Even so, if the tumor geometry and position are known by appropriate medical imaging techniques (e.g., MRI, CT), by using these models, it is possible to evaluate the outcome of the hyperthermia therapy's efficiency, also by taking into account the local features (e.g., tumor/tissue density, type and perfusion rate) and external factors (e.g., field amplitude and frequency) involved.

Acknowledgment

This work was supported by the Romanian PNII-26 NANOPART project.

References

[1] Q. A. Pankhurst, J. Connolly, S. K. Jones, and J. Dobson, "Applications of magnetic nanoparticles in biomedicine," *J. Phys. D: Appl. Phys.*, vol. 36, pp. R167–R181, 2003.

[2] R. Hergt, S. Dutz, R. Muller, and M. Zeisberger, "Magnetic particle hyperthermia: Nanoparticle magnetism and materials development for cancer therapy," *J. Phys: Condens. Matter*, vol. 18, pp. S2919–S2934, 2006.

[3] R. T. Gordon and J. R. Hines, "Intracellular hyperthermia: A biophysical approach to cancer treatment via intracellular temperature and biophysical alterations," *Medical Hypotheses*, vol. 5, p. 83, 1979.

[4] R. Hergt, W. Andra, C. G. d'Ambly, I. Hilger, W. A. Kaiser, U. Richter, and H. G. Schmidt, "Physical limits of hyperthermia using magnetite fine particles," *IEEE Trans. Magn.*, vol. 34, pp. 3745–3754, 1998.

[5] L. Y. Zhang, H. C. Gu, and X. M. Wang, "Magnetite ferrofluid with high specific absorption rate for application in hyperthermia," *J. Magn. Magn. Mater.*, vol. 311, pp. 228–233, 2007.

[6] S. Bae, S. W. Lee, Y. Takemura, E. Yamashita, J. Kunisaki, S. Zurn, and C. S. Kim, "Dependence of frequency and magnetic field on self-heating characteristic of $NiFe_2O_4$ nanoparticles for hyperthermia," *IEEE Trans. Magn.*, vol. 42, pp. 3566–3568, 2006.

[7] B. Payet, A. Siblini, M. F. Blanc-Mignon, and G. Noyel, "Comparison between a magneto-optical method and Fannin's technique for the measurement of Brown's relaxation frequency of ferrofluid," *IEEE Trans. Magn.*, vol. 35, pp. 2018–2023, 1999.

[8] I. A. Brezovich and R. F. Meredith, "Practical aspects of ferromagnetic thermoseed hyperthermia," *Radiol. Clin. North. Amer.*, vol. 27, pp. 589–602, 1989.

[9] R. Hergt and S. Dutz, "Magnetic particle hyperthermia—Biophysical limitations of a visionary tumour therapy," *J. Magn. Magn. Mater.*, vol. 311, pp. 187–192, 2007.

[10] M. Pavel, G. Gradinariu, and A. Stancu, "Study of the optimum dose of ferromagnetic nanoparticles suitable for cancer therapy using MFH," *IEEE Trans. Magn*, vol. 44, no. 11, pp. 3205–3208, 2008.

[11] COMSOL Multiphysics, Heat Transfer Module, User's Guide and Model Library pp. 145–161, pp. 243-264.

[12] H. H. Pennes, *J. Appl. Physiol*, vol. 1, p. 93, 1984.

[13] E. Y. K. Ng and N. M. Sudharsan, "Effect of blood flow, tumour and cold stress in a female breast: A novel time-accurate computer simulation," *J. Biomed. Eng.*, vol. 215, pp. 393–404, 2001.

[14] C. B. Saw, A. Loper, K. Komanduri, T. Combine, S. F. Huq, and C. Scicutella, "Determination of CT-to-density conversion relationship for image-based treatment planning systems," *Med. Dosim.*, vol. 30, pp. 145–148, 2005.

[15] J. A. Shepherd, K. M. Kerlikowske, R. Smith-Bindman, H. K. Genant, and S. R. Cummings, "Measurement of breast density with dual x-ray absorptiometry: Feasibility," *Radiology*, vol. 223, pp. 554–557, 2002.

[16] C. Sturesson and S. A. Engels, "A mathematical model for predicting the temperature distribution in laser-induced hyperthermia. Experimental evaluation and applications," *Phys. Med. Biol.*, vol. 40, pp. 2037–2052S, 1995.

[17] Z. Rumboldt, R. Al-Okaili, and J. P. Deveikis, "Perfusion CT for head and neck tumors: Pilot study," *Amer. J. Neuroradiol.*, vol. 26, pp. 1178–1185, 2005.

[18] M. Pavel and A. Stancu, "Study of the optimum injection sites for a multiple metastases region in cancer therapy by using MFH," *IEEE Trans. Magn.*, vol. 45, pp. 4825–4828, 2009.

[19] R. E. Rosensweig, "Heating magnetic fluid with alternating magnetic field," *J. Magn. Magn. Mater.*, vol. 252, pp. 370–374, 2002.